13

Double Hysteresis Loop in $BaTiO_3$-Based Ferroelectric Ceramics

Sining Yun
School of Material Science and Engineering, Xi'an University of Architecture and Technology, Xi'an, Shaanxi, China

1. Introduction

In 1951, the notion of anti-ferroelectricity based on the phenomenological theory was firstly proposed by C. Kittel (Kittel, 1951), and who predicted exist of the anti-ferroelectric materials and its some intrinsic characteristics. Subsequently, a double hysteresis (**P–E**) loop and a ferroelectric-antiferroelectric (FE-AFE) phase transition were observed in $PbZrO_3$ (Shirane et al., 1951, 1952) and Pb(Zr, Ti)O_3 (Sawaguchi, 1953) ceramics with a perovskite structure. Since then, the double hysteresis loop, one important macroscopic effect, has been regarded as a typical characteristic of antiferroelectric materials. This kinds of antiferroelectric behavior is also observed in Pb(Zr, Sn, Ti)O_3 and Pb(La, Zr, Sn, Ti)O_3 ceramics (Berlincourt, 1963, 1964; Biggers & Schulze, 1974; Gttrttritja et al., 1980; Shebanov et al., 1994).

Interestingly, the double hysteresis loops have been observed in $BaTiO_3$ (Merz, 1953), $BaTiO_3$-based (Ren, 2004; Zhang & Ren, 2005, 2006; Liu et al., 2006), $(Na_{0.5}Bi_{0.5})TiO_3$-based (Takenaka, 1991; Sakata & Masuda, 1974; Tu et al., 1994; Sakata et al., 1992), (Ba, Sr)TiO_3 (Zhang et al., 2004), $KNbO_3$ (Feng & Ren, 2007, 2008), $BiFeO_3$ (Yuen et al., 2007) and other lead-based perovskite ceramics such as Pb$(Yb_{0.5}Ta_{0.5})O_3$ (Yasuda & Konda, 1993), Pb$(Fe_{2/3}W_{1/3})O_3$-Pb$(Co_{1/2}W_{1/2})O_3$ (Uchino & Nomura, 1978), Pb$(Sc_{0.5}Ta_{0.5})O_3$ (Chu et al., 1993) and Pb$(Co_{1/2}W_{1/2})O_3$ (Hachiga et al., 1985) over the past decades. However, the observed double hysteresis loops have different physical origins.

For the physical origins of the double ***P-E*** loops observation in the perovskite structure materials, they can be generally classified into several groups below: (1) the double ***P-E*** loops result from antiferroelectric components. i.e., the observed double ***P-E*** loops in $PbZrO_3$ and Pb(Zr, Ti)O_3 ceramics. (2) the double ***P-E*** loops result from an electric field-induced antiferroelectric-to-ferroelectric phase transition as shown observed in Pb(La, Zr, Sn, Ti)O_3 ceramics. (3) two successive paraelectric-antiferroelectric-ferroelectric (***PE-AFE-FE***) phase transitions is often observed in highly ordered perovskite lead-based and lead-free complex compounds, and the double ***P-E*** loops are expected to accompany this phase transition. Such case often occur in Pb$(Yb_{0.5}Ta_{0.5})O_3$, Pb$(Fe_{2/3}W_{1/3})O_3$-Pb$(Co_{1/2}W_{1/2})O_3$, Pb$(Sc_{0.5}Ta_{0.5})O_3$ and Pb$(Co_{1/2}W_{1/2})O_3$ and $(Na_{0.5}Bi_{0.5})TiO_3$-based ceramics. (4) an aging effect far below Curie temperature (T_c) can induce the double ***P-E*** loops observation in many kind different compositional ceramics such as acctor-doped $BaTiO_3$ ceramics, Mn-

doped (Ba, Sr)TiO_3 ceramics, $KNbO_3$-based ceramics and $BiFeO_3$ ceramics. The aging-induced double ***P-E*** loops has been the highlights based on the high-quality publications and their cited times. (5) for the observed double ***P-E*** loops in $BaTiO_3$ crystals at the Curie point, its origin can not attributed to any one group mentioned above. The $BaTiO_3$ crystals go from a paraelectric to a ferroelectric state, while (Pb, Ba)ZrO_3 ceramics go from an antiferroelectric to a ferroelectric state when an electric field is applied. It is generally believed that the Curie point of the $BaTiO_3$ crystal shifts to higher temperature when a dc bias field is applied. The more detailed discussion about the origin of the double ***P-E*** loops in the $BaTiO_3$ crystal can consult the previous literatures titled "A theory of double hysteresis for ferroelectric crystals" (Srivastava, 2006).

After a brief review of the physical origin of double hysteresis loops in different perovskite structure ($A^+B^{5+}O_3$, $A^{2+}B^{4+}O_3$, $AA'BO_3$, $ABB'O_3$, etc) ceramic materials, this chapter begins with aging effect, namely a gradual change in physical properties with time. This is followed by discussions of the aging-induced double hysteresis loops in Bi doped (Ba, Ca)TiO_3 and Bi doped (Ba, Sr, Ca)TiO_3 ferroelectric ceramics. Some emphasis will be on the roles of acceptor-doping and donor-doping in understanding the physics of these materials.

2. Experimental procedures

2.1 Ceramics synthesis

A conventional solid reaction route was employed to synthesize ceramics samples. Reagent grade $BaCO_3$ (99.8%), Bi_2O_3 (99.8%), $SrCO_3$ (99.8%), $CaCO_3$ (99.8%) and TiO_2 (98%) as the raw materials were weighed according to the compositions $(Ba_{1-x}Ca_x)_{1-1.5y}Bi_yTiO_3$ (Bi-BCT, x =0.10, 0.20 and 0.30, y=0.05) and $(Ba_{1-x}Ca_{x/2}Sr_{x/2})_{1-1.5y}Bi_yTiO_3$ (Bi-BCST, x=0.10, 0.20 and 0.40, y=0 and 0.05). $(Ba_{0.925}Bi_{0.05})(Ti_{0.90}Ca_{0.10})O_3$ (designated hereafter Bi-BTC) was prepared to compare the effect of Ca substitution at the Ti sites of Bi-BCT. After ball-milled in alcohol for 6 h using agate balls in a planetary mill, the slurry was dried, and then calcined at 1100 ^{o} C for 4-5h. The calcined powder was ball milled and dried again to obtain homogeneous powder. Pellets of 10 mm in diameter and ~1 mm thick were pressed using 5 % PVA binder. Slow heating at 500 ^{o}C for 3-4h burned out the binder. The samples were sintered at 1240 ^{o}C -1300^{o}C in air for 3 h, with heating rates of 200^{o}C/h. The samples were cooled with the furnace.

2.2 Characterizations

The phase structures of the ceramics at different temperature were checked by the X-ray powder diffraction (XRD, D/Max2200 RZGAKV: Rigaku Inc.D, Japan) on an automated Rigaku D/max 2400 X-ray diffractometer with rotating anode using CuK_α radiation. The microstructures were examined by a scanning electron microscopy (SEM, Quanta 200 FEG System: FEI Co., USA) with X-ray energy dispersive spectroscopy (EDS) for chemical analysis. Raman scattering investigation was performed at room temperature by using an ALMEGA dispersive Raman spectrometer (ALMEGA, Therm Nicolet, Madison,WI).

2.3 Property measurements

After polishing, the dimensions were measured before silver electrodes were deposited on the pellets, then the specimens were fired at 810 ^{o}C for 10 mins. Dielectric properties at

frequencies ranging from 0.1kHz to 100 kHz were measured with an Agilent 4284A LCR meter, as samples were heated at a rate of 2 °C/min from negative 80 to positive 200 °C. Hysteresis loops were measured in a wide temperature range using a computer-controlled, modified Sawyer-Tower circuit at frequency of 1 Hz. Current-field relation was measured on an automatic ferroelectric test system of aixACT TF-ANALY2ER2000. Applied electric field signal is triangular, and a period time is a second.

3. Results and discussion

3.1 Structural analysis

It has been reported that the solubility limit of Bi is around 5 at. % in $BaTiO_3$ (Zhou et al., 1999), and around 10 at. % in $(Ba_{0.2}Sr_{0.8})TiO_3$ (Zhou et al., 2000), respectively. Moreover, 5 at. % of Bi doping can be fully incorporated into the perovskite lattice of $Ba_{1-x}Sr_xTiO_3$ ($x < 0.80$) (Zhou et al., 2001). It is then possible to assume that 5 at. % of Bi doping can be fully incorporated into the perovskite lattice of $(Ba_{1-x}Ca_x)TiO_3$ (Bi-BCT, x=0.10, 0.20 and 0.30) and $(Ba_{1-x}Ca_{x/2}Sr_{x/2})TiO_3$ (Bi-BSCT, x=0.10, 0.20 and 0.40). XRD analysis confirmed this assumption. Fig. 1 show the XRD patterns of 5 at. % of Bi doped $(Ba_{1-x}Ca_x)TiO_3$ ceramics. The XRD patterns of all the compositions showed mainly a single perovskite phase.

The structural evolution of Bi-doped BCST ceramics samples from x=0.10 to 0.40 is shown in Fig. 2. The XRD results of 5 at. % Bi-doped BCST are consistent with those of $(Ba_{1-x}Sr_x)_{1-1.5y}Bi_yTiO_3$ (Zhou et al., 2001) and Bi-BCT, showing that they are a single phase. The crystalline symmetry of Bi-doped BCST ceramics is a rhombohedral for x=0.40. However, it tends appreciably towards the tetragonal for x=0.20. The rhombohedral phase is illustrated by the increased splitting between the (021) and (003) peaks in two-theta near 39° while the tetragonal phase is illustrated by the increased splitting between the (002) and (200) peaks in two-theta near 45°. There are splits in the peaks observed at two-theta of about 39° and 45°, respectively, as shown in Fig.3, indicating the coexistence of the tetragonal and rhombohedral phases of Bi-BCST for x=0.10 and that of Bi-BCT for x=0.10 and 0.20.

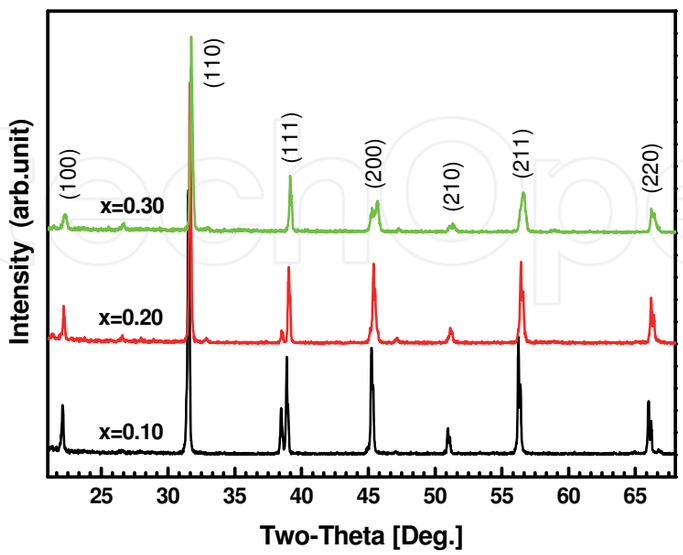

Fig. 1. XRD patterns of Bi-BCT ceramics with different compositions (x=0.10, 0.20 and 0.30, y=0.05).

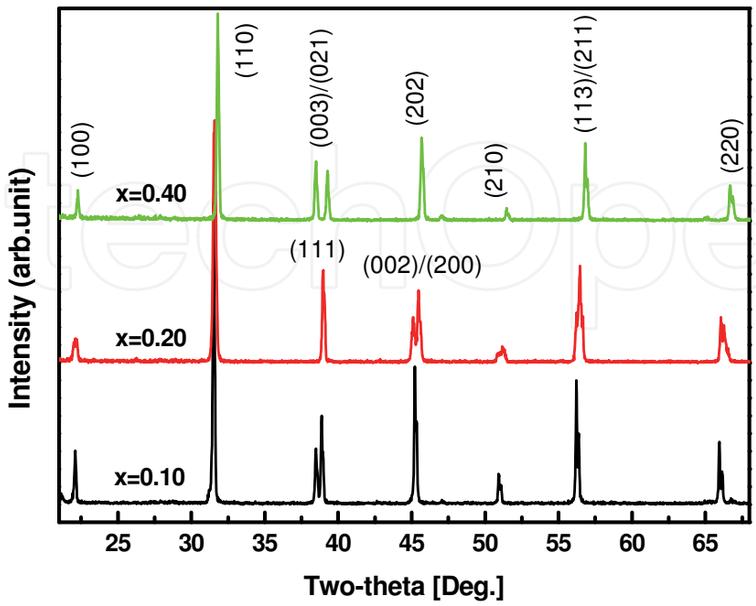

Fig. 2. XRD patterns of Bi-BSCT ceramics with different compositions (x=0.10, 0.20 and 0.40, y=0.05).

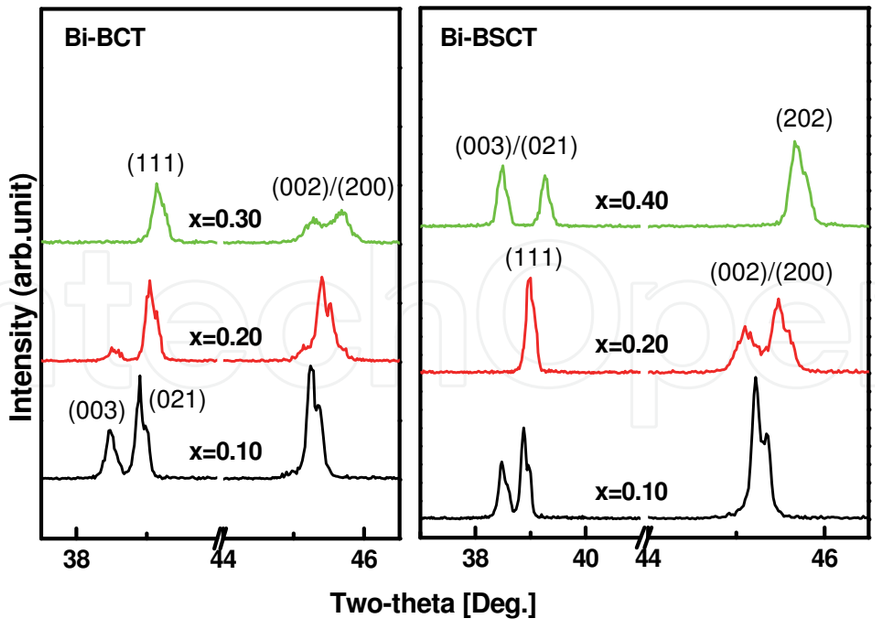

Fig. 3. Enlarged XRD patterns of Bi-BCT and Bi-BSCT(y=0.05) ceramics with different compositions with two-theta value ranging from 37.5° to 46.5°.

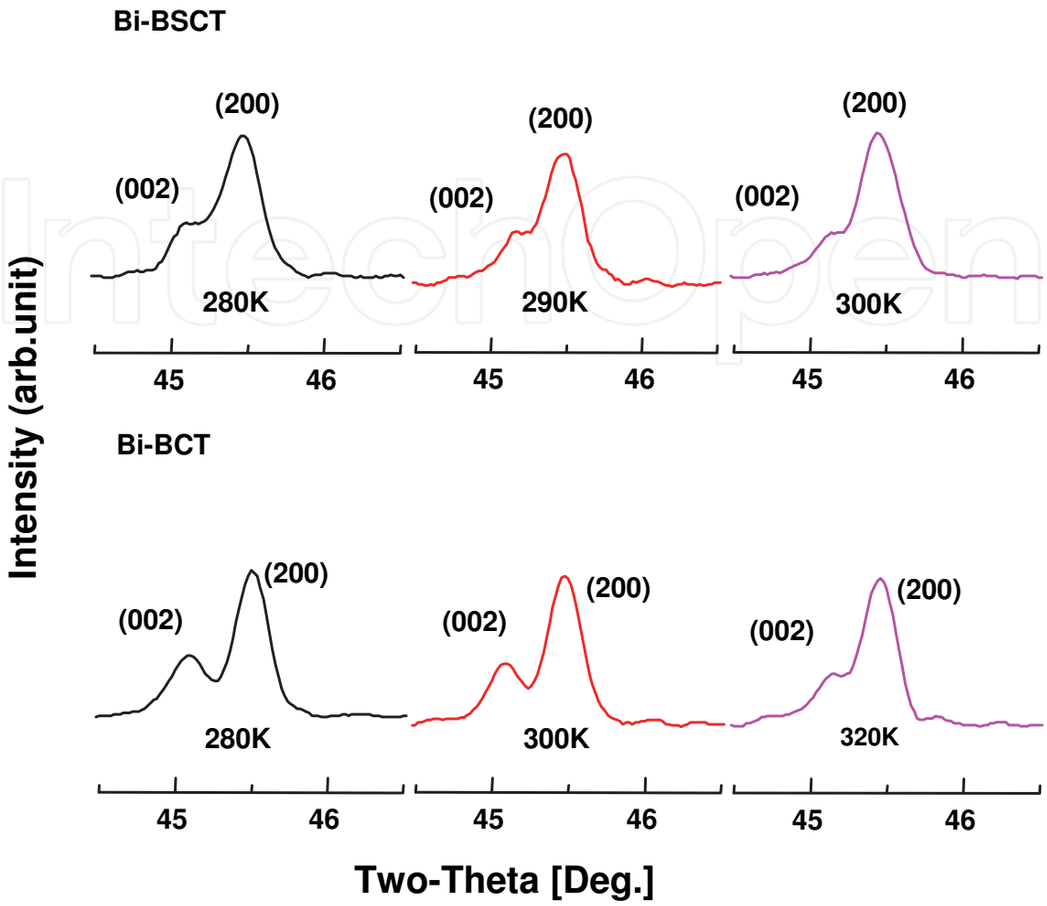

Fig. 4. Changes in the (002)/(200) reflection of XRD patterns of Bi-BCT and Bi-BSCT (x=0.10, y=0.05) ceramics with different temperatures.

To check the crystal symmetry, X-ray powder diffraction (XRD) at different temperatures was performed for Bi-BCT and Bi-BSCT (x=0.10, y=0.05). Fig. 4 shows the form of one of the structure sensitive maxima in the XRD patterns. It is found from the changes in the (002)/(200) refection with temperature that Bi-BCT ceramics have a tetragonal structure throughout the whole temperature range from 280 K up to 320 K while Bi-BSCT ceramics have a tetragonal structure throughout the whole temperature range from 280 K up to 300 K.

3.2 Ferroelectric properties

Fig. 5 and Fig. 6 show the plots of polarization ***P*** vs electrical field ***E*** (***P-E***) at elevate temperature for Bi-BCT and Bi-BCST (x=0.10 and 0.20, y=0.05), respectively. A well-behaved hysteresis loop can be observed at 280 K for Bi-BCT (x=0.10 and 0.20). When the temperature was increased, the double hysteresis loop, typical of antiferroelectric materials, was observed at 300 K for Bi-BCT and at 280 K for Bi-BSCT, with a nearly linear ***P-E*** relationship at the mid-part of the hysteresis loop. With further increased temperature, hysteresis could not be detected, the ***P-E*** loops were slim and showed dielectric quasilinearity over a wide electric field range.

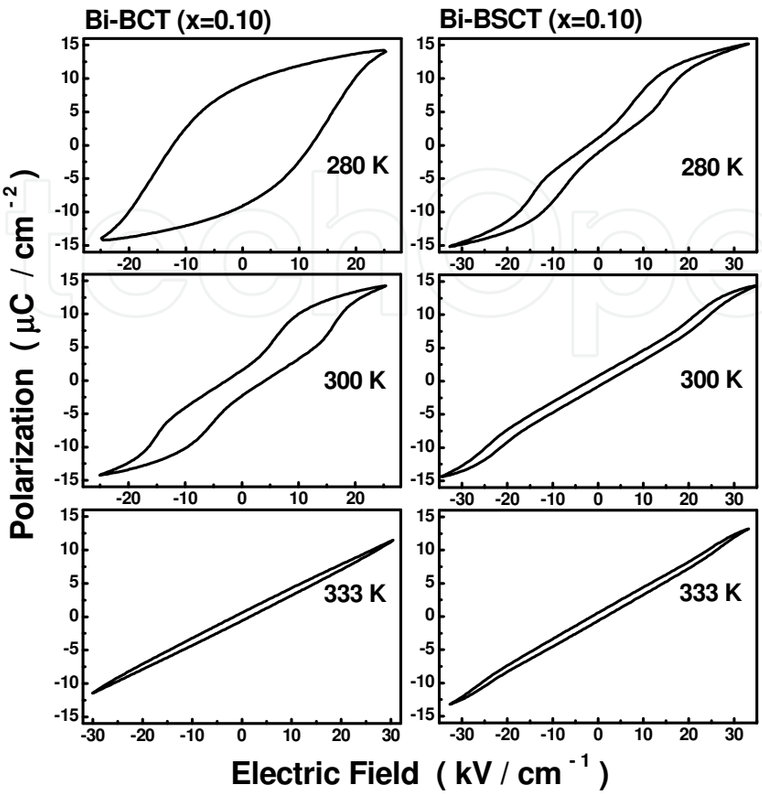

Fig. 5. The electrical field (**E)** dependence of polarization (**P)** at elevated temperature measured at 1 Hz for Bi-BCT and Bi-BSCT (x=0.10,y=0.05).

Note that a remarkable double-like ***P-E*** loop is not observed for Bi-BCT (x=0.30). However, the ***E*** dependence of ***P*** and current density (***J***) **(J-E)** relationships have shown that four remarkable ***J*** peaks are observed for Bi-BCT (x=0.30), indecating of the existence of double-like ***P-E*** loop for x=0.30 in Bi-BCT. Talking about that the present chapter foucses on the double ***P-E*** loops in Bi-BCT and Bi-BSCT ceramics, the related data for **J-E** relationship are not shown here.

The ***P-E*** loops transform from the normal hysteresis loop to an interesting double-like hysteresis loop, and then to the nearly linear one with increasing temperature. These characteristics obtained from the loops at elevated temperature suggest that different ferroelectric behaviors have occurred in Bi-BCT. It seems that two successive paraelectric-antiferroelectric-ferroelectric (***PE-AFE-FE***) phase transitions exist in Bi-BCT ceramics. By contrast, this similar transform from the normal to the double to the quasilinear can not be detected in Bi-BSCT ceramics. Polarization data at a lower temperature could not be obtained for Bi-BSCT ceramics due to the limitation of the present measuring equipment. However, one can assume that an ferroelectric–antiferroelectric transformation occurs at a lower temperature (temperature is less than 280 K) for Bi-doped BCST ceramics. This assumption needs to be confirmed experimentally. The appropriate research is now being carried out.

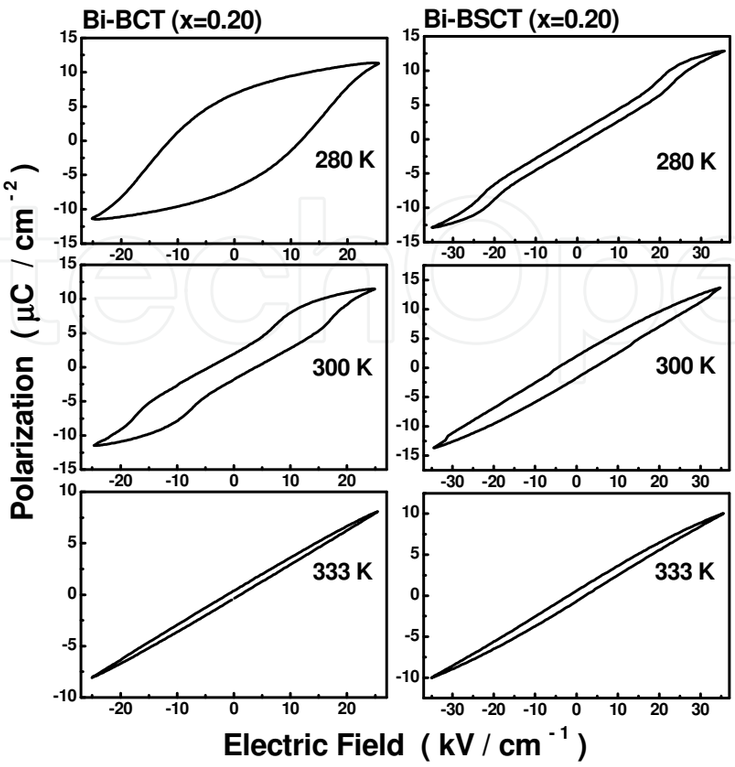

Fig. 6. The electrical field (**E**) dependence of polarization (**P**) at elevated temperature measured at 1 Hz for Bi-BCT and Bi-BSCT (x=0.20,y=0.05).

A linear dielectric response is observed for Bi-BCT and Bi-BSCT, that is, the ***P-E*** relationship is close to linear, unlike that for normal ferroelectrics and lead-based relaxors. The quasi-linear ***P-E*** relationship looks somewhat similar to that taken on the antiferroelectric sample. In this case, the linear ***P-E*** dependence is typical for antiferroelectric materials. In order to demonstrate that dielectric quasi-linearity in a certain electric field range is a typical antiferroelectric behavior or not, a complete investigation including the electric field-induced and temperature-induced structure phase transition has been performed in our previous literatures.

3.3 Dielectric properites

The temperature dependence of the dielectric constant and the dielectric loss of Bi-BCT and Bi-BSCT ceramics for different frequencies are shown in Fig. 7(A)-(D). The dielectric constant has a broad maximum at a temperature of the peak dielectric constant (T_m). T_m increases with increasing frequency. For example, T_m is equal to 341 K at 1 kHz and 347 K at 1 MHz for Bi-BCT (x=0.10), respectively. With decreasing temperature, the value of dielectric loss increases rapidly around the temperature of the dielectric loss. With increasing frequencies, the peak dielectric constant decreases and T_m shifts to high temperature. Such change trends of the dielectric constant and the dielectric loss with the frequencies and the temperatures is a type of dielectric relaxation behavior, which has been reported in detail in the solid state physics text book.

The possible mechanism for the relaxor behavior observation in Bi-doped $SrTiO_3$ (Ang et al., 1998), Bi-doped $Ba_{1-x}Sr_xTiO_3$ (Zhou et al., 2001), Ca-doped $SrTiO_3$ (Bednorz & Müller, 1984) and Li-doped $KTaO_3$ (Toulouse et al., 1994) has been discussed in detail in the previous publications. A widely accepted viewpoint is that the dielectric relaxation behavior in these systems was due to a random electric field induced ferroelectric domain state. According to their viewpoint, the Bi^{3+} ions which substitute for A-site ions in BCT and BCST ceramics can also be located at off-center positions and A-site vacancies may also appear to compensate for the charge misfit arising from the A-site ions substituted by Bi^{3+} ions. A random electric field formed by off-center Bi^{3+} ions and Bi^{3+}–V''_A dipoles would then suppress the ferroelectricity of BCT and BCST and result in the relaxor behavior observed for Bi-doped BCT and BCST. If Ca^{2+} ions can locate at B-sites like Ti^{4+} ions, to balance the charge misfit, a next-neighbor oxygen can be vacant, and form a Ca^{2+}–V_O neutral center. Such Ca^{2+}–V_O centers form dipoles and thus set up local electric fields, which suppress the ferroelectricity of BCT and BCST and result in the relaxor behavior observed in BCT and BCST.

In most cases of ferroelectric phase transition, where the new ordered phase originates from structural changes, there will be a peak in the dielectric spectrum but not all peculiarities or peaks correspond to a structural phase transition. For example, All classical relaxors, such as $Pb(Mg_{1/3}Nb_{2/3})O_3$ (PMN) and low x $(1-x)Pb(Mg_{1/3}Nb_{2/3})O_3$-$xPbTiO_3$ (Bokov & Ye, 2006), show the dielectric peaks but do not undergo the ferroelectric (or antiferroelectric) phase transition. Therefore, the dielectric peak may only indicate the possible phase transition. If the ***FE-AFE-PE*** transition has occurred in Bi-BCT, there will be two corresponding dielectric peak in the dielectric spectrum. However, the dielectric spectrum of Bi-BCT and Bi-BSCT show only one peak at temperature ranging from 190 K to 428 K as seen in Fig.7.

On the other hand, there is no direct indication of the appearance of antiferroelectric components in $(Ba,Ca)TiO_3$ (Han et al., 1987; Zhuang, et al., 1987; Mitsui & Westphal, 1961; Baskara & Chang, 2003). Therefore, the aging-induced effect should be responsible for the double ferroelectric hysteresis observation in Bi-BCT and Bi-BSCT ceramics.

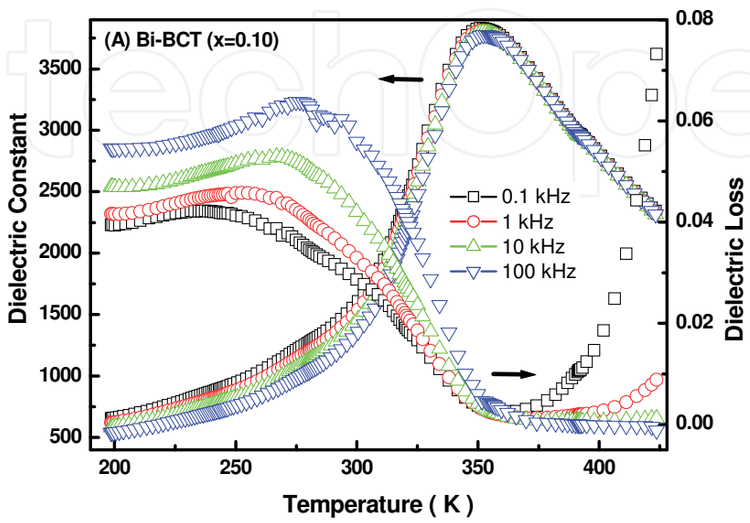

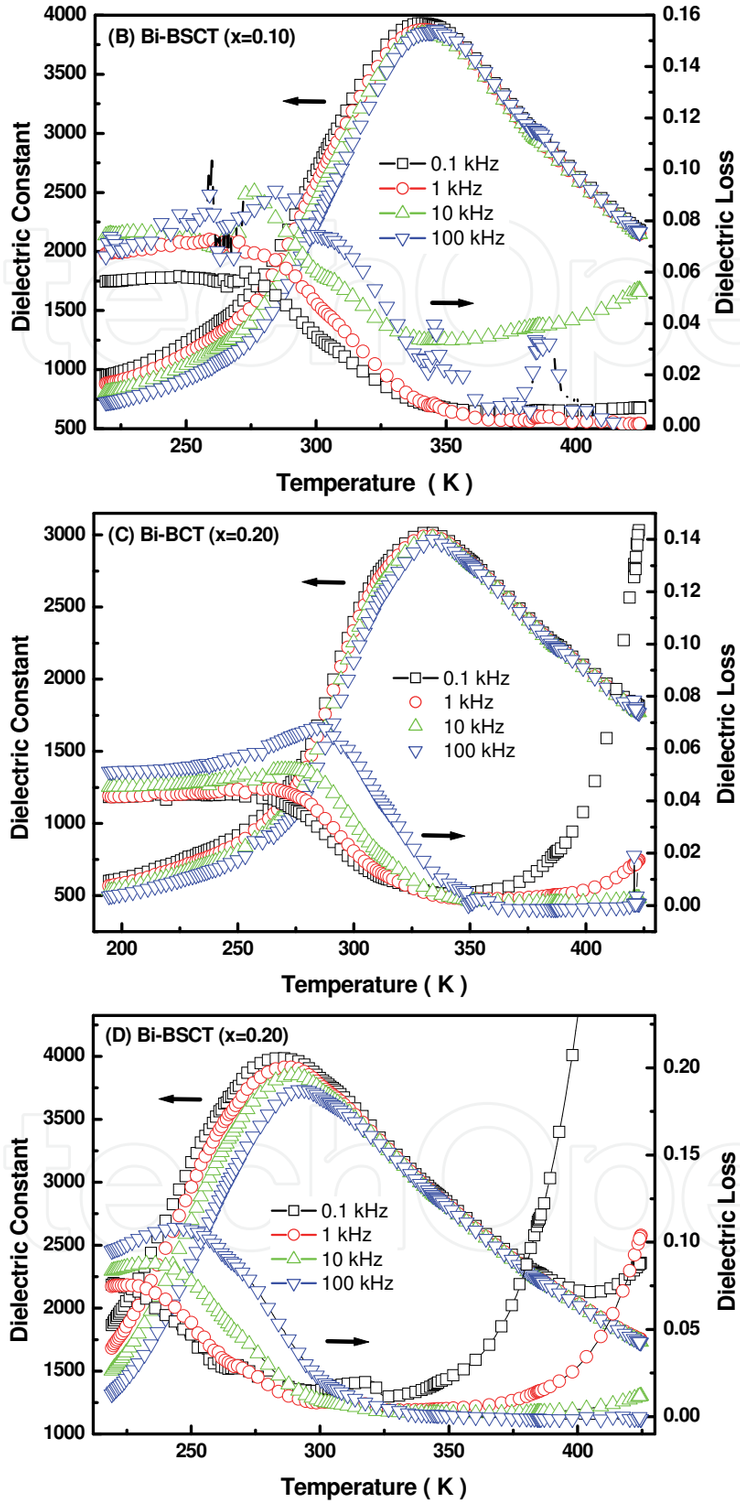

Fig. 7. Temperature dependence of the dielectric constant and the dielectric loss of Bi-BCT and Bi-BSCT for x=0.10 ((A) and (B)), x=0.20 ((C) and (D)) and y=0.05 at 0.1, 1, 10, 100 kHz (for dielectric constant, from top to bottom, for dielectric loss, from bottom to top).

3.4 Ferroelectric aging effect

The interesting aging-induced double ***P-E*** hysteresis loop was also reported in various ferroelectric systems. Many mechanisms such as the grain boundary effect (Karl & Hardtl, 1978), the domain-wall pinning effect (Postnikov et al, 1970), the volume effect (Lambeck & Jonker, 1986) and symmetry-conforming short range ordering (SC-SRO) mechanism of point defects (Ren, 2004; Zhang & Ren, 2005, 2006; Liu et al., 2006) have been proposed to explain this phenomenon. Although all these models seem to be able to provide a self-consistent explanation of the double hysteresis loop in aged ferroelectric crystals, the grain boundary effect cannot explain the perfect double ***P-E*** loop exists in the aged single-crystal sample, the domain-wall pinning effect cannot explain the restoration of the initial multidomain state from a single-domain state because there would be no domain wall to be dragged back, and the volume effect is based on a key assumption that there exist dipolar defects and they follow spontaneous polarization after aging (Zhang & Ren, 2005, 2006). Compared all these models, SC-SRO mechanism, which also is a volume effect, provides a microscopic explanation for the origin of aging, and it involves no assumption. The conformation of the defect dipole with spontaneous polarization naturally comes from the symmetry-conforming property of the defects. Generally, all these models agree that defects play a decisive role in the aging induced phenomena. However, they differ much in the driving force for defect migration.

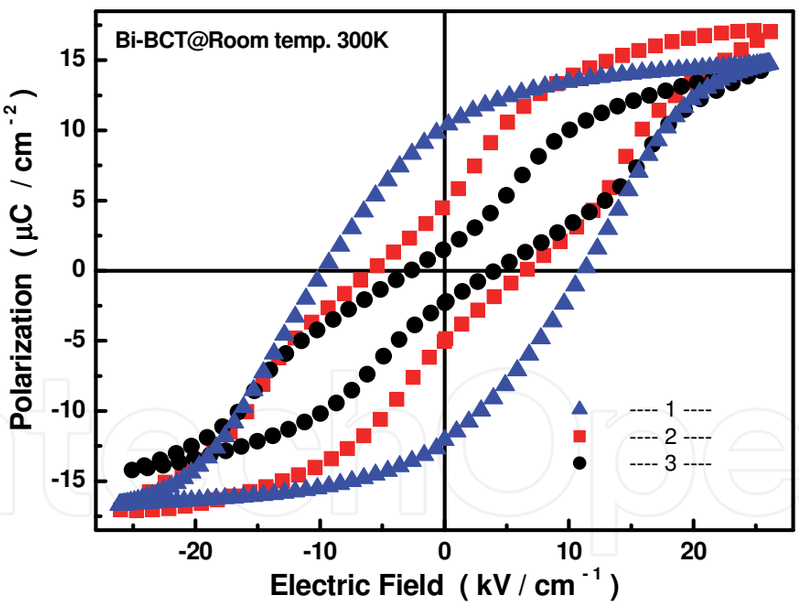

Fig. 8. Hysteresis loops for fresh and aged Bi-BCT (x=0.10) ceramic samples at room temperature of 300 K. (1—Fresh or deaged ; 2—A shorter period of aging; 3—A longer period of aging).

To check further whether there is a diffusional aging effect, the samples were "de-aged" by holding them at 470 K for 1 h, followed by a quick cooling to room temperature above Curie temperature. The room temperature hysteresis loops were measured simultaneously. Fig. 8 shows the experimental results of the hysteresis loops for the Bi-BCT in de-aged (fresh) and

aged state, respectively. The de-aged sample shows a normal hysteresis loop, but all the aged samples show interesting double hysteresis loops. The change from the single ***P-E*** loops in the de-aged sample to the double ***P-E*** loops in the aged sample should exclude antiferroelectric components and any electric field-induced ***PE-FE*** phase transition near Curie temperature. It indicates that the aging effect must be responsible for the double ***P-E*** loops observed in Bi-BCT.

3.5 Raman analysis

The aging effect in acceptor-doped ferroelectrics is generally considered to be due to the migration of oxygen vacancies (which are highly mobile) during aging (Ren, 2004; Zhang & Ren, 2005, 2006; Liu et al., 2006; Zhang et al., 2004; Feng & Ren, 2007, 2008). However, the O^{2-} vacancies in our Bi-BCT and Bi-BSCT samples were not formed artificially by substitution of lower-valence ions for Ti ions on the B-sites. To understand the aging effect in Bi-BCT, we need to analyze its defect structure. For Bi doped BCT and BSCT with the ABO_3 pervoskite structure [$(Ba_{0.90}Ca_{0.10})_{0.925}Bi_{0.05}TiO_3$ and $(Ba_{0.90}Sr_{0.05}Ca_{0.05})_{0.925}Bi_{0.05}TiO_3$], there are two possible vacancies: first, the Bi^{3+} ions substituted for A-site divalent ions (Ba^{2+}, Sr^{2+} or/and Ca^{2+}) in BCT and BSCT can be located at off-center positions of the A-site, so that A-site vacancies are formed to compensate the charge imbalance arising from the substitution, and second, that Ca^{2+} ions substitute for Ti^{4+} ions in BCT, and cause the formation of O^{2-} vacancies to balance the charge misfit. The previous experimental results from equilibrium electric conductivity (Han et al., 1987), scanning electric microscopy (Zhuang, et al., 1987), neutron diffraction (Krishna et al, 1993) and Raman and dielectric spectroscopies (Zhuang, et al., 1987; Chang & Yu, 2000; Park et al., 1993), have given evidence that a small amount of Ca^{2+} ions can substitute for Ti^{4+} ion causing the formation of O^{2-} vacancies to balance the charge misfit, although the ionic radius and chemical valence of the Ca^{2+} ions is very different from those of the Ti^{4+} ions. 4 mol% Ca^{2+} ions were found to have substituted for the Ti^{4+} ions even when the molar ratio of (Ba+Ca)/Ti was 1 for the starting materials used by Krishna et al. in their studies of $Ba_{0.88}Ca_{0.12}TiO_3$ samples prepared by the solid-state reaction technique. Following the above-mentioned suggestion, it seems that substitution of the Ca^{2+} ions for the Ti^{4+} ions had occurred in the Bi-BCT and Bi-BSCT ceramics prepared by the solid-state reaction technique.

Since aging is controlled by the migration of mobile oxygen vacancies, an experimental study of the formation of O^{2-} vacancies in Bi-BCT by Raman scattering at room temperature was performed with the results shown in Fig. 9. (Ba0.925Bi0.05)(Ti0.90Ca0.10)O2.90 (Bi-BTC) ceramics were prepared in order to compare the effect of Ca substitution at the Ti sites of Bi-BCT. In single crystal and ceramic samples of $BaTiO_3$, almost the same Raman bands, such as those at 165 cm^{-1} [A(TO)], 173 cm^{-1} (mixed modes), 266 cm^{-1} [A(TO)], 306 cm^{-1} [E(TO)], 470 cm^{-1} [E(T)+A(L)], 516 cm^{-1} [A(T)] and 712 cm^{-1} [A(LO)+E(LO)], were observed (Burns, 1974; Begg et al., 1996). Very similar results were also observed in $(Ba_{1-x}Ca_x)TiO_3$ and $BaTi_{1-y}Ca_yO_3$ ceramics (Chang & Yu, 2000). For A-site substitution, with increasing x, the Raman bands related to the phonon vibration of the Ba-O bonds shift to higher frequency (512 and 719 cm^{-1} for x = 0.005, 521 and 730 cm^{-1} for x = 0.20) while the Raman bands caused by the phonon vibration of the Ti-O bonds shift to lower frequency (259 and 306 cm^{-1} for x = 0.005, 248 and 298 cm^{-1} for x = 0.20). For B-site substitution, Ba-O bonds are closely related to the formation of the 517 and 718 cm^{-1} bands, and Ti-O bonds are closely related to the formation of the 257

and 307 cm^{-1} bands in $BaTi_{1-y}Ca_yO_3$. Fig.9 shows the bands 299, 520 and 723 cm^{-1} were independent of the formation of Ca_{Ba} and Ca_{Ti} in Bi-BCT and Bi-BTC. From these results we can conclude that Ba-O bonds are closely related to the formation of the 520 and 723 cm^{-1} bands, and Ti-O bonds to the formation of the 262 and 299 cm^{-1} bands. We also find the development of a weak new Raman band at 827cm^{-1} for Bi-BTC and Bi-BCT (see Fig. 9). Almost the same Raman bands (832 cm^{-1}) have been observed in $Ba(Ti_{0.985}Ca_{0.005}Nb_{0.01})O_3$ and $BaTi_{1-y}Ca_yO_3$ (y=0.005 and 0.015) ceramics (Chang & Yu, 2000). This higher frequency Raman band has resulted from the formation of Ca_{Ti} defects. That is, Ca^{2+} ion substitution for B-site Ti^{4+} ions has occurred in Bi-BCT, and O^{2-} vacancies have formed to compensate for the charge imbalance. The present results give critical evidence for the formation of O^{2-} vacancies.

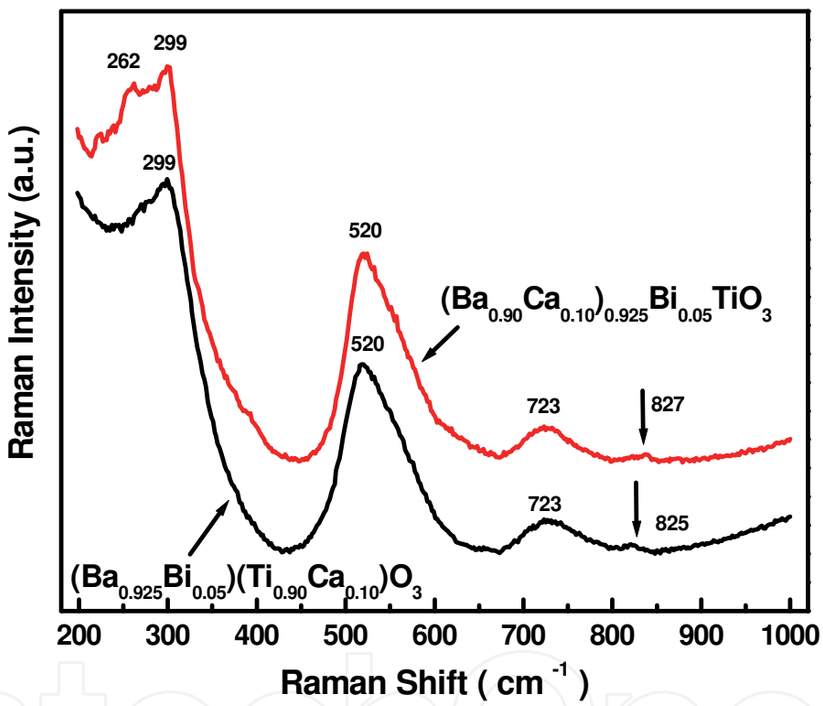

Fig. 9. Raman spectra of the Bi-BCT and Bi-BTC ceramics at room temperature.

3.6 Origin of double-like P-E loops in Bi-BCT and Bi-BSCT

As mentioned above, there are two kinds of vacancy, A-site vacancies and oxygen vacancies, around an acceptor Ca^{2+} ion. Considering the mobility of oxygen vacancies and the immobility of cation vacancies at ordinary temperatures, the observation of double ***P-E*** loops in Fig. 8 can be explained by a special aging effect related to the defect symmetry defined as the conditional probability of finding O^{2-} vacancies at site *i* (*i*=1–6) of an ABO_3 single cell (Ren, 2004; Zhang & Ren, 2005, 2006; Liu et al., 2006; Zhang et al., 2004; Feng & Ren, 2007, 2008). Fig. 10 depicts how the double ***P-E*** loops are produced in a single-crystal grain of the aged Bi-BCT sample. The high-temperature sintering gives the oxygen and cation vacancies sufficient mobility. Thus, in the paraelectric phase, the probability of

finding an O^{2-} vacancy and a A-site vacancy around an acceptor Ca^{2+} ion will adopt a cubic symmetry, according to the SC-SRO mechanism of point defects [Fig. 10(d)] (Ren, 2004).

For the de-aged tetragonal samples, which are formed by immediately cooling from the paraelectric state at 470 K down to 300 K, the SRO distribution of point defects retains the same cubic symmetry as that in the cubic paraelectric phase because the diffusionless paraeletric-ferroelectric transition cannot alter the original cubic SRO symmetry of point defects (Ren, 2004). As a result, the de-aged ferroelectric state has tetragonal crystal symmetry, but cubic defect symmetry; thus the two symmetries do not match [see Fig. 10(a)]. According to the SC-SRO mechanism (Ren, 2004; Zhang & Ren, 2005, 2006; Liu et al., 2006; Zhang et al., 2004; Feng & Ren, 2007, 2008), such a state [Fig. 10(a)] is unstable due to the mismatch between the defect symmetry and the crystal symmetry. After aging for a long time, the defect symmetry in each domain follows the polar tetragonal crystal symmetry and exhibits a defect dipole moment following the polarization direction of the residing domain. Every domain is in its stable state, as shown in Fig. 10(b). The SRO symmetry of O^{2-} vacancies around the Ca^{2+} ion can be gradually changed into a polar tetragonal symmetry (which produces a defect dipole $\boldsymbol{P_D}$) [see Fig. 10(b) and 10(e)] by the migration of mobile O^{2-} vacancies, which is the same process as for the acceptor-doped case (Ren, 2004; Zhang & Ren, 2005, 2006; Liu et al., 2006; Zhang et al., 2004; Feng & Ren, 2007, 2008). However, the SRO symmetry of A-site vacancies around Ca^{2+} the ion still remains cubic because the cation vacancies are immobile at such temperatures (Tan et al., 1999) [Fig. 10(b) and 10(f)]. When an electric field is applied to the naturally aged tetragonal Bi-BCT sample, $\boldsymbol{P_S}$ is switched to the field $\boldsymbol{E}$ direction while $\boldsymbol{P_D}$ keeps its original direction during such a sudden process [Fig. 10(b) to 10(c)]. Therefore, after removing the electric field [Fig. 10(c) to 10(b)], the unchanged defect symmetry and the associated $\boldsymbol{P_D}$ cause reversible domain switching. As a consequence, the original domain pattern is restored [Fig. 10(b)] so that the defect symmetry and dipole moment follow the crystal symmetry in every domain. An interesting double hysteresis loop in the ***P-E*** relation for Bi-BCT is expected to accompany this reversible domain switching, as observed in Fig. 8. Clearly, the explanation is the same as that for acceptor-doped ABO_3 ferroelectrics (Ren, 2004; Zhang & Ren, 2005, 2006), since aging originates from the mismatch between the defect symmetry and the crystal symmetry after a structural transition. Comparing the double ***P-E*** loop "2" with "3" in Fig. 8, it can be seen that the naturally aging-induced double loop is obvious if the Bi-BCT samples are given a longer period of aging (33 months), which indicates that a longer time was required to establish an equilibrium defect state at room temperature (300 K).

When the measurement temperature is reduced to 280 K from 300 K, the double ***P-E*** loop becomes a normal one. The change of shape of the ***P-E*** loops in Fig. 5 and Fig. 6 can be explained as follows: normally, the coercive field increases with decreasing temperature, especially in some lead-based ceramic samples (Chu et al., 1993; Sakata, et al., 1992). When the samples were measured at low temperature, the coercive field may become higher than the driving force for reversible domain switching. As a result, the $\boldsymbol{P_D}$ creating the driving force is not enough to switch a reversible domain and thus result in a single ***P-E*** loop observation at low temperature for Bi-BCT. A similar change from double to single ***P-E*** loops with temperature has been observed in specially aged $KNbO_3$-based ceramics (Feng & Ren, 2007).

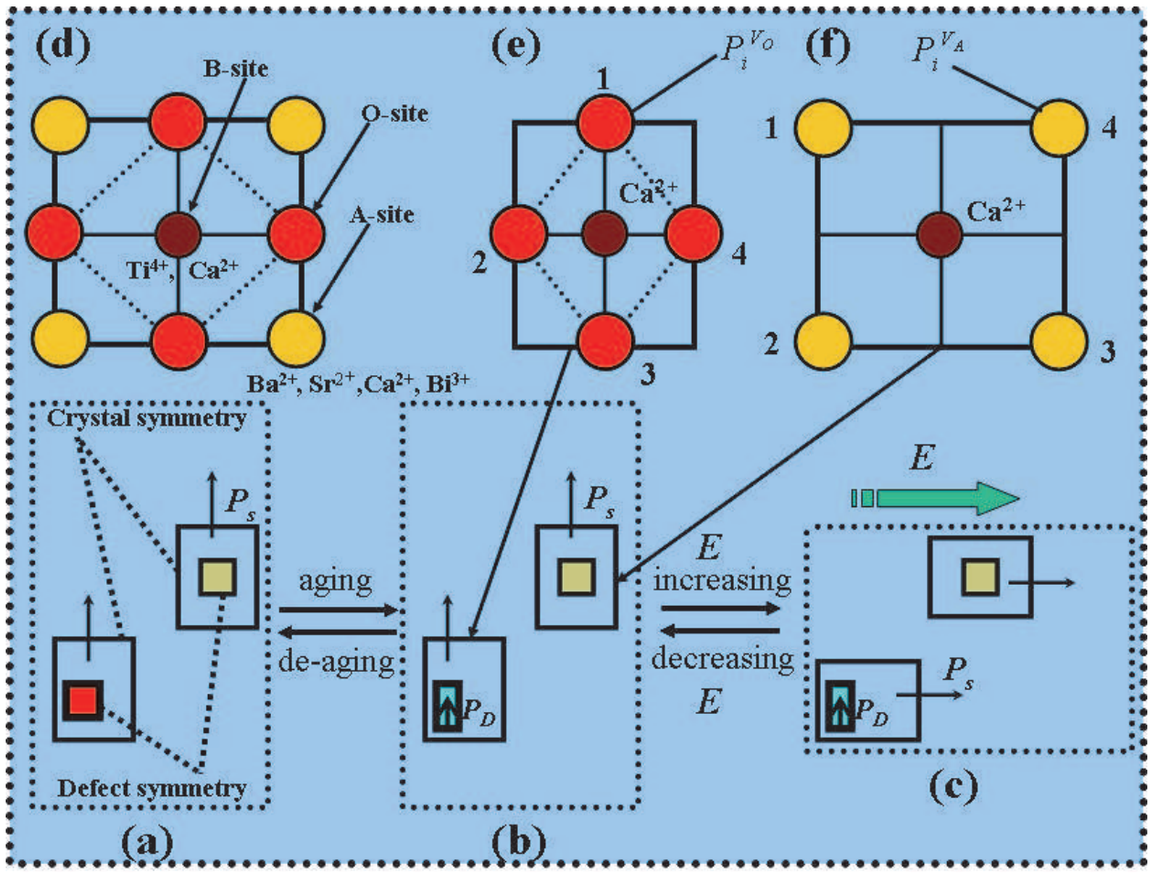

Fig. 10. Microscopic explanation for double-like ***P-E*** loops in bismuth doped BCT ceramics based on the SC-SRO principles. (a) When samples were cooled down below T_C after deaging, the crystal changes to the ferroelectric state with a spontaneous polarization P_S due to the relative displacement of positive and negative ions. The defect symmetry is cubic while the crystal symmetry is tetragonal. (b) After aging, the defect symmetry around an acceptor ion (Ca^{2+}) adopts a polar tetragonal symmetry with a defect dipole P_D, and the defect symmetry of cation vacancies still keeps cubic. (c) On increasing electric field, P_S rotates but P_D keeps the original orientation; this unswitched P_D provides a driving force for the reversible domain switching to (b). (d) When samples was de-aged above the phase transition point T_C, the SRO distribution of point defects keeps the cubic symmetry, oxygen vacancies keep $P_1^{V_O} = P_2^{V_O} = P_3^{V_O} = P_4^{V_O}$ and cation vacancies keep $P_1^{V_A} = P_2^{V_A} = P_3^{V_A} = P_4^{V_A}$, the crystal is in the paraelectric state and has a cubic symmetry. (e)-(f) After natural aging to establish an equilibrium defect state, the redistribution of oxygen vacancies makes $P_1^{V_O} > P_2^{V_O} = P_4^{V_O} > P_3^{V_O}$ [see (e)] while cation vacancies keep $P_1^{V_A} = P_2^{V_A} = P_3^{V_A} = P_4^{V_A}$ because of their immobility (see (f)]. Large rectangle represents crystal symmetry while the small black rectangle represents an oxygen SRO symmetry around an acceptor defect; the gray square represents the SRO of A-site vacancy around an acceptor defect. P_S refers to spontaneous polarization and P_D refers to defect polarization. $P_i^{V_O}$ is the conditional probability of oxygen vacancy occupying O^{2-} site i (i=1–4) next to a given Ca^{2+} and Sr^{2+}, and $P_i^{V_A}$ is the conditional probability of finding a cation vacancy (A-site vacancy) at site i (i=1–4) around Ca^{2+} and Sr^{2+}.

The above results describing the natural aging effect in $(Ba_{1-x}Ca_x)_{0.925}Bi_{0.05}TiO_3$ ferroelectrics are very similar to the special aging effect in acceptor-doped $BaTiO_3$ materials (Ren, 2004; Liu et al., 2006; Zhang et al., 2004; Feng & Ren, 2007; Yuan et al., 2007). The interesting double ***P-E*** loop behavior between the natural aging effect of ABO_3 compound with A-site substitution and the special aging effect of ABO_3 compound with B-site substitution can be explained by the SC-SRO mechanism of point defects. As discussed above, such a mechanism relies essentially on symmetry, not on the crystal structure or ionic species. The key idea of the SC-SRO mechanism is that an equilibrium defect state tends to adopt a match between the defect symmetry and the crystal symmetry in every domain. This tendency does not depend on the crystal structure or ionic species (Ren, 2004; Liu et al., 2006; Zhang et al., 2004; Feng & Ren, 2007, 2008; Yuan et al., 2007).

It seems from the change of shape of hysteresis loops that these two ceramic samples undergo a ferroelectric-antiferroelectric-paraelectric (***FE-AFE-PE***) transition, similar to that observed in $(Na_{0.5}Bi_{0.5})TiO_3$-based ceramics (Takenaka, 1991; Sakata & Masuda, 1974; Tu et al., 1994; Sakata et al., 1992). Some researchers thought that an intermediate phase with double hysteresis loops is as proof of an additional antiferroelectric transition (Sakata & Masuda, 1974; Tu et al., 1994; Balashova & Tagantsev, 1993). Indeed, heterophase fluctuations proposed between the paraelectric and the ferroelectric phase are unreasonable because of energy considerations, but it is possible that at a higher temperature there occurs an extra local phase transition to a nonpolar state. The energy gap between this phase and the ferroelectric phase is relatively small, and therefore heterophase fluctuations between the two phases can take place (Uchino & Nomura, 1978). Inhomogeneities due to chemical disorder cause nonuniformity in the free energy of the two states throughout the material, increasing the probability of heterophase fluctuations. For the selected samples Bi-BSCT, disordering in the Ba, Sr, Ca and Bi cations distributed in A-sites will be favorable for increasing the fluctuation probability, and resulting in an intermediate phase with double hysteresis loops between the paraelectric and the ferroelectric phase. However, it has not been confirmed by other experimental measurements whether the intermediate phase exists in Bi-BSCT. Further experiments on Bi-BCT and Bi-BSCT with TEM for observing the intermediate phase transition need to be carried out.

Here, we need to mention that $BaTiO_3$ ferroelectric systems with dielectric relaxation behavior can usually be formed by doping point defects (impurity or doping) into a normal ferroelectric system. Bi-doped BCST is in such case. These random point defects distort the surrounding crystal lattice and thus generate random local fields. The random distribution of local fields brings about significant effects: the long-range ordering of electric dipoles is prohibited or destroyed while the local short-range ordering is retained. In simpler language, the random point defects will crush the macro-size domains into nano-size domains. Thus, only the local ordered polar nano-domain exists in Bi-doped BCT and BCST. The nearly linear ***P-E*** response (see also Fig. 5 and Fig. 6) is due to the random local field, stemming from the lattice defects by dopants, which has a strong frustration to the nano-domains. This has contributed significantly to our understanding of the contradictions between high dielectric constant and dielectric linearity in the most relaxors. In addition, the linear dielectric response in solid solutions with the dielectric relaxation behavior may provide possibilities for applications.

It is clear that an aging effect exists in Bi-BCT ceramics in the present report, so does it in the more complicated compositions Bi-BSCT ceramics. Based on the SC-SRO mechanism, the diffusional age-induced effect is the main reason causing the double hysteresis loops

observed in Bi-BCT. Similarly, the double hysteresis loops observed between the paraelectric and the ferroelectric states for Bi-BSCT ceramics can be also explained by a point-defect-mediated reversible domain switching mechanism. However, talking about the complexity of ceramic compositions, it is unclear whether the aging effect is only reason resulting in the observed double hysteresis loops for Bi-BCT and Bi-BSCT ceramics according to the suggestion mentioned above, which needs to be confirmed by further experimental evidence.

4. Conclusion

$(Ba_{1-x}Ca_x)_{1-1.5y}Bi_yTiO_3$ (Bi-BCT, x =0.10, 0.20 and 0.30, y=0.05), $(Ba_{1-x}Ca_{x/2}Sr_{x/2})_{1-1.5y}Bi_yTiO_3$ (Bi-BCST, x=0.10, 0.20 and 0.40, y=0 and 0.05) and $(Ba_{0.925}Bi_{0.05})(Ti_{0.90}Ca_{0.10})O_3$ (Bi-BTC) perovskite ceramics were prepared through solid-state reaction technique. The structural, dielectric and ferroelectric properties and ferroelectric aging effect of Bi-BCT and Bi-BSCT ceramics were investigated.

5 at. % of Bi doping can be fully incorporated into the perovskite lattice of Bi-BCT and Bi-BSCT ceramics. The crystalline symmetry of Bi-BCT and Bi-BCST ceramics is a rhombohedral phase for x=0.40 while it is the tetragonal phase for x=0.30, and the crystalline symmetry of ceramics samples tends appreciably towards the coexistence of the tetragonal and rhombohedral phases for Bi-BCT (Bi-BCST) with the compositions of x=0.10 and x=0.20. XRD patterns at elevated temperature has demonstrated that the (002)/(200) refection of Bi-BCT can keep spliting throughout the whole temperature range from 280 K up to 320 K while that of Bi-BSCT can keep spliting throughout the whole temperature range from 280 K up to 300 K.

A typical relaxor behavior, a similar behavior to lead-based relaxor ferroelectrics, has been observed in Bi-BCT and Bi-BSCT ceramics. A random electric field is suggested to be responsible for the relaxor behavior observations. The dielectric peak corresponding to the ferroelectric-antiferroelectric transition cannot be found in the dielectric spectrum within the temperature range 198 K to 430 K for Bi-BCT and Bi-BSCT.

The ***P-E*** relationship at elevated temperature shows that an abnormal double-like ***P-E*** loop was observed for Bi-BCT and Bi-BSCT. The de-aging experiment has shown that there is a diffusional aging effect in Bi-BCT ceramics. The change from the single ***P-E*** loops in the de-aged sample to the double ***P-E*** loops in the aged sample excludes the existence of ferroelectric-antiferroelectric transition in Bi-BCT. Raman scattering gives critical evidence for the formation of O^{2-} vacancies in Bi-BCT. A point-defect-mediated reversible domain switching mechanism is suggested to be responsible for the double hysteresis loops observed between the paraelectric and the ferroelectric states for Bi-BCT ceramics. It is expected that the abnormal ferroelectric behavior of Bi-BSCT ceramics can be explained using a point-defect-mediated reversible domain switching mechanism. The striking similarity of the aging effect between nonequivalence substitution for A-site ions and B-site ions of ABO_3 systems indicates a common physical origin of aging.

5. Acknowledgment

The author acknowledges the financial support of the Scientific Research Program Funded by Shaanxi Provincial Education Department (Program No.2010JK655). This work was also

supported by the PUNAI Education Scholarship through PuYang Refractory Group Co., Ltd. (PRCO).

6. References

Kittel, C. (1951). Theory of Antiferroelectric Crystals. *Physical Review,* Vol.82, No.5, (June 1951), pp. 729–732

Shirane, G.; Sawaguchi, E. & Takagi, Y. (1951). Dielectric Properties of Lead Zirconate. *Physical Review,* Vol.84, No.3, (June 1951), pp. 476–481

Shirane, G. (1952). Ferroelectricity and Antiferroelectricity in Ceramics $PbZrO_3$ Containing Ba or Sr. *Physical Review,* Vol.86, No.2, (June 1952), pp. 219-227

Sawaguchi, E. (1953). Ferroelectricity versus Antiferroelectricity in the Solid Solutions of $PbZrO_3$ and $PbTiO_3$. *Journal of the Physical Society of Japan,* Vol.8, No.5, (September 1953), pp. 615-629

Berlincourt, D.; Jaffe, H.; Krueger, H. H. A.; & Jaffe, B. (1963). Release of Electric Energy in $PbNb(Zr,Ti,Sn)O_3$ by Temperature and by Pressure-enforced Phase Transitions. *Applied Physics Letters*, Vol.3, No.5, (September 1963), pp. 90-92

Berlincourt, D.; Krueger, H. H. A.; & Jaffe, B. (1964). Stability of Phases in Modified Lead Zirconate with Variation in Pressure, Electric Field, Temperature and Composition. *Journal of Physics and Chemistry of Solids,*Vol.25, No.7, (July 1964), pp. 659-674

Biggers, J. V. & Schulze, W. A. (1974). Direct Current Bias of Antiferroelectric PLZT Ceramics. *American Ceramic Society Bulletin,* Vol.53, No.11, (July 1974), pp. 809-812

Gttrttritja, T. R.; Kumarakrishuau, S. & Subbarao, E. C. (1980). Modified PLZT High Voltage Dielectrics. *Ferroelectrics*, Vol.27, No.1, (January 1980), pp. 277-280

Shebanov, L.; Kusnetsov, M. & Sternberg, A. (1994). Electric Field-Induced Antiferroelectric-to-Ferroelectric Phase Transition in Lead Zirconate Titanate Stannate ceramics Modified wtih Lanthanum. *Journal of Applied Physics*, Vol.76, No.7, (October 1994), pp. 4301-4304

Merz, W. J. (1953). Double Hysteresis Loop of $BaTiO_3$ at the Curie Point. *Physical Review,* Vol.91, No.3, (August 1953), pp. 513-517

Ren, X. (2004). Large Electric-Field-Induced Strain In Ferroelectric Crystals by Point-Defect mediated Reversible Domain Switching. *Nature Materials*, Vol.3, (Feburary 2004), pp. 91–94

Zhang, L. & Ren, X. (2005). In Situ Observation of Reversible Domain Switching in Aged Mn-Doped $BaTiO_3$ Single Crystals. *Physical Review B*, Vol.71, No.17, (May 2005), pp. 174108

Zhang, L. & Ren, X. (2006). Aging Behavior in Single-Domain Mn-Doped $BaTiO_3$ Crystals: Implication for A Unified Microscopic Explanation of Ferroelectric Aging. *Physical Revuew B*, Vol.73, No.9, (March 2006), pp. 094121

Liu, W.; Chen, W.; Yang, L.; Zhang, L.; Wang, Y.; Zhou, C.; Li, S. & Ren, X. (2006). Ferroelectric Aging Effect in Hybrid-doped $BaTiO_3$ Ceramics and the Associated Large Recoverable Electrostrain. *Applied Physics Letters*, Vol.89, No.17, (October 2006), pp. 172908

Takenaka, E.; Maruyama, K. I. & Sakata, K. (1991). $(Bi_{1/2}Na_{1/2})TiO_3$-$BaTiO_3$ System for Lead-free Piezoelectric Ceramics. *Japanese Journal of Applied Physics*, Vol.30, No.9B, (September 1991), pp. 2236-2239

Sakata, K. & Masuda, Y. (1974). Ferroelectric and Antiferroelectric Properties of $(Bi_{1/2}Na_{1/2})TiO_3$-$SrTiO_3$ Solid Solution Ceramics. *Ferroelectrics*, Vol.7, No.1, (January 1974), pp. 347-349

Tu, C. S.; Siny, I. G. & Schmidt, V. H. (1994) Sequence of Dielectric Anomalies and High-Temperature Relaxation Behavior in $Na_{1/2}Bi_{1/2}TiO_3$. *Physical Revuew B*, Vol.49, No.13, (April 1994), pp. 11550.

Sakata, K.; Takenaka, T. & Naitou, Y. (1992). Phase Relations, Dielectric and Piezoelectric Properties of Ceramics in the System $Na_{1/2}Bi_{1/2}TiO_3$–$PbTiO_3$. *Ferroelectrics*, Vol.7, No.1, (January 1992), pp. 219-349

Zhang, L.; Chen, W. & Ren, X. (2004). Large Recoverable Electrostrain in Mn-doped (Ba, Sr)TiO_3 Ceramics. *Applied Physics Letters*, Vol.85, No.23, (October 2004), pp. 5658-5660

Feng, Z. & Ren, X. (2007). Aging Effect and Large Recoverable Electrostrain in Mn-doped $KNbO_3$-based Ferroelectrics. *Applied Physics Letters*, Vol.91, No.3, (July 2007), pp. 032904

Feng, Z. & Ren, X. (2008). Striking Similarity of Ferroelectric Aging Effect in Tetragonal, Orthorhombic and Rhombohedral Crystal Structures. *Physical Revuew B*, Vol.77, No.13, (April 2008), pp. 134115

Yuen, G. L.; Yang, Y. & Or, S. W. (2007). Aging-Induced Double Ferroelectric Hysteresis Loops in $BiFeO_3$ Multiferroic Ceramic. *Applied Physics Letters*, Vol.91, No.12, (September 2007), pp. 122907

Yasuda, N. & Konda, J. (1993). Successive Paraelectric-Antiferroelectric-Ferroelectric Phase Transitions in Highly Ordered Perovskite Lead Ytterbium Tantalite. *Applied Physics Letters*, Vol.62, No.5, (Feburary 1993), pp. 535-537

Uchino, K. & Nomura, S. (1978). Dielectric and Magnetic Properties in the Solid Solution System $Pb(Fe_{2/3}W_{1/3})O_3$-$Pb(Co_{1/2}W_{1/2})O_3$. *Ferroelectrics*, Vol.17, No.1, (January 1978), pp. 505-510

Chu, F.; Setter, N. & Tagantsev, A. K. (1993). The Spontaneous Relaxor-Ferroelectric Transition of $Pb(Sc_{0.5}Ta_{0.5})O_3$. *Journal of Applied Physics*, Vol.74, No.8, (October 1993), pp. 5129-5134

Hachiga, T.; Fujimoto, S. & Yasuda, N. (1986). Temperature and Pressure Dependence of the Dielectric Properties of $Pb(Co_{1/2}W_{1/2})O_3$. *Journal of Physics D: Applied Physics*, Vol.19, No.2, (Feburary 1986), pp. 291-298

Srivastava, N. & Weng, G. J. (2006). A Theroy of Double Hysteresis for Ferroelectric Crystals. *Journal of Applied Physics*, Vol.99, No.5, (March 2006), pp. 054103

Zhou, L.; Vilarinho, P. M. & Baptista, J. L. (1999). Solubility of Bismuth Oxide in Barium Titanate. *Journal of the American Ceramic Society,* Vol.82, No.4, (April 1999), pp. 1062-1066

Zhou, L.; Vilarinho, P. M. & Baptista, J. L. (2000). Relaxor Behavior of $(Sr_{0.8}Ba_{0.2})TiO_3$ Ceramic Solid Solution Doped with Bismuth. *Journal of Electroceramic,* Vol.5, No.3, (May 2000), pp. 191-199

Zhou, L.; Vilarinho, P. M. & Baptista, J. L. (2001). Dielectric Properties of Bismuth Doped $Ba_{1-x}Sr_xTiO_3$ Ceramics. *Journal of the European Ceramic Society,* Vol.21, No.4, (April 2001), pp. 531-534

Ang, C.; Yu, Z.; Vilarinho, P. M. & Baptista, J. L. (1998). Bi:$SrTiO_3$: A Quantum Ferroelectric and a Relaxor. *Physical Revuew B*, Vol.57, No.13, (April 1998), pp. 7403-7406

Bednorz, J. G. & Müller, K. A. (1984). $Sr_{1-x}Ca_xTiO_3$: An XY Quantum Ferroelectric with Transition to Randomness. *Physics Review Letters*, Vol.52, No.25, (June 1984), pp. 2289-2292

Toulouse, J.; Vugmeister, B. E. & Pattnaik. (1994).Collective Dynamics of Off-Center Ions in $K_{1-x}Li_xTaO_3$: A Model of Relaxor Behavior. *Physics Review Letters*, Vol.73, No.25, (December 1994), pp. 3467-3470

Bokov, A. A. & Ye, Z. G. (2006). Recent Progress in Relaxor Ferroelectrics with Perovskite Structure. *Journal of Materials Science,* Vol.41, No.1, (January 2006), pp. 31-52

Han, Y. H.; Appleby, J. B. & Smyth, D. M. (1987). Calcium As An Acceptor Impurity in $BaTiO_3$. *Journal of the American Ceramic Society,* Vol.70, No.2, (Feburary 1987), pp. 96-100

Zhuang, Z. Q.; Harmer, M. P.; Smyth, D. M. & Newnham, R. E. (1987). The Effect of Octahedrally-Coordinated Calcium on the Ferroelectric Transition of $BaTiO_3$. *Materials Research Bulletin,* Vol.22, No.10, (October 1987), pp. 1329-1335

Mitsui, T. & Westphal, W. B. (1961). Dielectric and X-ray Studies of $Ca_xBa_{1-x}TiO_3$ and $Ca_xSr_{1-x}TiO_3$. *Physical Review,* Vol.124, No.5, (July 1961), pp. 1354-1359

Baskara, N. & Chang, H. (2003).Thermo-Raman and Dielectric Constant Studies of $Ca_xBa_{1-x}TiO_3$ Ceramics. *Materials Chemistry and Physics,* Vol.77, No.3, (January 2003), pp. 889-894

Karl, K & Hardtl, K. H. (1978). Electrical After-Effects in Pb(Ti, Zr)TiO_3 Ceramics. *Ferroelectrics*, Vol.17, No.1, (January 1978), pp. 473-486

Postnikov, V. S.; Pavlov, V. S. & Turkov, S. K. (1970). Internal Friction in Ferroelectrics Due to Interaction of Domain Boundaries and Point Defects. *Journal of Physics and Chemistry of Solids,* Vol.31, No.8, (August 1970), pp. 1785-1791

Lambeck, P. V. & Jonker, G. H. (1986). The Nature of Domain Stabilization in Ferroelectric Perovskites. *Journal of Physics and Chemistry of Solids,* Vol.47, No.5, (September 1986), pp. 453-461

Krishna, P. S. R.; Pandey, D.; Tiwari, V. S.; Chakravarthy, R. & Dasannachary, B. A. (1993). Effect of Powder Synthesis Procedure on Calcium Site Occupancies in Barium Calcium Titanate: A Rietveld analysis. *Applied Physics Letters*, Vol.62, No.3, (January 1993), pp. 231-233

Chang, M. C. & Yu, S. C. (2000). Raman study for $(Ba_{1-x}Ca_x)TiO_3$ and $Ba(Ti_{1-y}Ca_y)O_3$ crystalline ceramics. *Journal of Materials Science Letters,* Vol.19, No.15, (August 2000), pp. 1323-1325

Park, J. G.; Oh, T. S. & Kim, Y. H. (1992). Dielectric Properties and Microstructural Behaviour of B-Site Calcium-Doped Barium Titanate Ceramics. *Journal of Materials Science,* Vol.27, No.21, (November 1992), pp. 5713-5719

Burns, G. (1974). Lattice Modes In Ferroelectric Perovskites. II. $Pb_{l-x}Ba_xTiO_3$ Including $BaTiO_3$. *Physical Revuew B*, Vol.10, No.5, (September 1974), pp. 1951-1959

Begg, B. D.; Finnie, K. S. & Vance, E. R. (1996). Raman Study of the Relationship between Room-Temperature Tetragonality and the Curie Point of Barium Titanate. *Journal of the American Ceramic Society,* Vol.79, No.10, (October 1996), pp. 2666-2672

Tan, Q.; Li, J. & Viehland, D. (1999). Role of Lower Valent Substituent-Oxygen Vacancy Complexes in Polarization Pinning in Potassium-Modified Lead Zirconate Titanate. *Applied Physics Letters*, Vol.75, No.3, (May 1999), pp. 418-420

Balashova, E. V. & Tagantsev, A. K. (1993). Polarization Response of Crystals with Structural and Ferroelectric Instabilities. *Physical Revuew B*, Vol.48, No.14, (October 1993), pp. 9979-9986

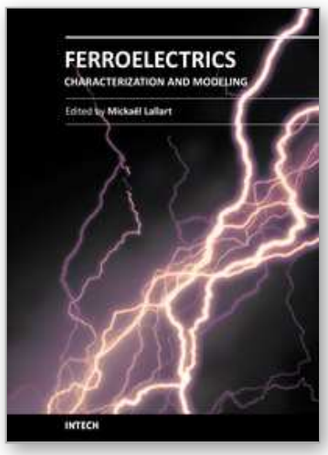

Ferroelectrics - Characterization and Modeling

Edited by Dr. MickaÃ«l Lallart

ISBN 978-953-307-455-9
Hard cover, 586 pages
Publisher InTech
Published online 23, August, 2011
Published in print edition August, 2011

Ferroelectric materials have been and still are widely used in many applications, that have moved from sonar towards breakthrough technologies such as memories or optical devices. This book is a part of a four volume collection (covering material aspects, physical effects, characterization and modeling, and applications) and focuses on the characterization of ferroelectric materials, including structural, electrical and multiphysic aspects, as well as innovative techniques for modeling and predicting the performance of these devices using phenomenological approaches and nonlinear methods. Hence, the aim of this book is to provide an up-to-date review of recent scientific findings and recent advances in the field of ferroelectric system characterization and modeling, allowing a deep understanding of ferroelectricity.

INTECH
open science | open minds

InTech Europe
University Campus STeP Ri
Slavka Krautzeka 83/A
51000 Rijeka, Croatia
Phone: +385 (51) 770 447
Fax: +385 (51) 686 166
www.intechopen.com

InTech China
Unit 405, Office Block, Hotel Equatorial Shanghai
No.65, Yan An Road (West), Shanghai, 200040, China
中国上海市延安西路65号上海国际贵都大饭店办公楼405单元
Phone: +86-21-62489820
Fax: +86-21-62489821

IntechOpen